Northumbria Research Link

Citation: Emran, Mohammed Y., Shenashen, Mohamed A., Elmarakbi, Ahmed, Selim, Mahmoud M. and El-Safty, Sherif A. (2022) Nitrogen-doped carbon hollow trunk-like structure as a portable electrochemical sensor for noradrenaline detection in neuronal cells. Analytica Chimica Acta, 1192. p. 339380. ISSN 0003-2670

Published by: Elsevier

URL: https://doi.org/10.1016/j.aca.2021.339380 <https://doi.org/10.1016/j.aca.2021.339380>

This version was downloaded from Northumbria Research Link: https://nrl.northumbria.ac.uk/id/eprint/48134/

Northumbria University has developed Northumbria Research Link (NRL) to enable users to access the University's research output. Copyright © and moral rights for items on NRL are retained by the individual author(s) and/or other copyright owners. Single copies of full items can be reproduced, displayed or performed, and given to third parties in any format or medium for personal research or study, educational, or not-for-profit purposes without prior permission or charge, provided the authors, title and full bibliographic details are given, as well as a hyperlink and/or URL to the original metadata page. The content must not be changed in any way. Full items must not be sold commercially in any format or medium without formal permission of the copyright holder. The full policy is available online: http://nrl.northumbria.ac.uk/policies.html

This document may differ from the final, published version of the research and has been made available online in accordance with publisher policies. To read and/or cite from the published version of the research, please visit the publisher's website (a subscription may be required.)

Northumbria University NEWCASTLE

University Library

Nitrogen-doped carbon hollow trunk-like structure as a portable electrochemical sensor for noradrenaline detection in neuronal cells

M. Y. Emran[a], M. A. Shenashen[a], A. Elmarakbi[b], M. M. Selim[c], S. A. El-Safty [a,*]

[a] National Institute for Materials Science (NIMS), Research Center for Functional Materials, 1-2-1 Sengen, Tsukuba-shi, Ibaraki-ken 305-0047, Japan

[b] Faculty of Engineering and Environment, Northumbria University, Newcastle upon Tyne, NE1 8ST, UK

[c] Al-Aflaj College of Science and Human Studies, Prince Sattam Bin Abdulaziz University, Al-Aflaj, 710-11912, Saudi Arabia

*Correspondence: sherif.elsafty@nims.go.jp

Homepage: https://samurai.nims.go.jp/profiles/sherif_elsafty

Abstract

To date, the production and development of portable analytical devices for environmental and healthcare applications are rapidly growing. Herein, a portable electrochemical sensor for monitoring of noradrenaline (NA) secreted from living cells using mesoporous carbon-based materials was fabricated. The modification of the interdigitated electrode array (IDA) by nitrogen-doped mesoporous carbon spheres (N-doped MCS) and nitrogen-doped carbon hollow trunk-like structure (N-doped CHT) was used to fabricate the NA sensor. The N-doped CHT surface shows multiple holes distributed with micrometer-sized open holes (1–2 μm) and nanometer-sized thin walls (~98 nm). The N-doped CHT surface heterogeneity of wrinkled and twisted hollow trunk structures improve the diffusion pathway and the NA molecules loading. The N-doped CHT/IDA showed a highly selective assay for monitoring of NA with high sensitivity (1770 μA/μM×cm^2), a low detection limit

(0.005 µM), and a wide linear range (0.01–0.3 µM). The N-doped CHT/IDA monitored the NA secreted from PC12 cells under various concentrations of simulation agents (KCl). The designed N-doped CHT/IDA provides a portable NA-sensor assay with facile signaling, good stability, high biocompatibility, in-vitro assay compatibility, and good reproducibility. Therefore, the designed sensor can be used as a portable sensor for NA detection in live cells and can be matched with portable smartphones after further developments.

Keyword; Portable electrochemical sensor; Noradrenaline; In-Vitro assay; Alzheimer diseases; PC12; Porous N-doped carbon materials.

1. Introduction

Catecholamines (adrenaline, noradrenaline (NA), and dopamine (DA)) are biogenic amines present in the central nervous system and act as neurotransmitters. These biomolecules play a vital role in signaling transmission and further biological activity in the human body [1-4]. NA is one of the catecholamines produced from the adrenal gland and nerve tissue [4]. The effects of NA can be observed on various biological functions and human health activities, such as heart rate, blood glucose level, blood vessels, muscle activity, and fight/flight actions [5-7]. In addition, NA acts as an alpha receptor and is present in arteries [8].

The fluctuation in NA levels serves as a biomarker of psychiatric disorders, such as dementia, Alzheimer's, and Parkinson's disease [9-11]. NA is used to manage several diseases, including hypotension, cardiac disease, anxiety, and diabetes [12-14]. In this respect, scholars focus on a highly sensitive protocol for identifying NA in various biological samples (i.e., human fluids and brain samples) for therapeutic and neurological applications.

Monitoring of NA has been conducted using various analytical methods, such as fluorescence microscopy [15-17], ultra-performance liquid chromatography-tandem mass spectrometry [18], and electrochemistry [7, 11, 19]. These methods suffer from disadvantages, including the pretreatment of samples, requirement of highly specialized

equipment, and long-term need for highly qualified technicians. Most of these disadvantages can be resolved by electrochemical methods involving rapid reactions, easy processing, no sample pretreatment, use of handheld devices, ease of use, and applicability in in vitro and in vivo tests [20-23]. Point-of-care-based devices have been widely designed for the production of portable biosensors [20, 24]. The highly sensitive and selective quantification of NA in neural models of neuronal cells/neural tissues, brain samples, and human fluids remains a challenge. Various approaches have been developed to overcome these limitations by producing highly active materials that convert the NA signal with high sensitivity and selectivity [7, 11, 14, 19, 25]. The modified electrodes of conducting polymer [14], metal oxides such as NiO [11], nanocomposites [26, 27], carbon-based electrodes [7, 19, 28], and treated and modified multi-walled carbon nanotubes (MWCNTs) [29] have been used for the detection of NA. The designed materials surface structure, size, and composition play an important role in the biomolecules sensing such as NA. Most of these materials need sophisticated preparation procedures, multiple treatment process, fabrication limitations of mechanical and thermal stabilities, low biocompatibility, and high cytotoxicity for further applications in in-vivo applications, and lack of sensitivity and selectivity [30, 31]. Therefore, we aimed to synthesis an electrode material that overcome most of these limitations with beneficial advantages of i) economic benefits, ii) easy processing, iii) high electrochemical behavior, iv) solid mechanical and thermal stability, and v) intense sensing properties. Besides, the development of highly sensitive and selective approaches for in-situ biomolecular monitoring remains a challenge.

Carbon-based materials with multi-function heteroatom centers can be candidate catalysts because of their numerous active centers, high structural stability, low cost, high mechanical and thermal stability, excellent electron mobility, fast load transport, and outstanding resilience [32, 33]. Heteroatom doping of graphene and MWCNTs has been widely used for various heterogeneous catalysts and biosensing applications [32, 34, 35]. Graphene and MWCNTs are highly ordered structures that limit the active doping by heteroatoms (N, P, S, and B) in the carbon framework and active functional sites [32].

Doped carbon-based materials with heteroatoms of P, N, S, and B have been recognized as highly functional carbon materials with high electrical conductivity and highly active centers. [32, 36-38]. Heteroatoms and carbon atoms form new bonds and functionality, change the bond lengths, and create an atomic charge density between carbon and doping heteroatoms. New carbon-based materials are designed with high electrochemical performance, including fast charge transport, facile binding to targets, and high electron/molecular diffusion [32, 36]. The presence of N atoms in the graphitic carbon chain breaks the carbon electroneutrality and creates abundant active sites with a partially polarized surface of positive and negative charges. This functionality arises from the difference in the electronegativity and electron configuration between N and C atoms [39, 40]. Thus, the preparation of N-doped carbon-based materials with a novel procedure, porous network, high surface area, long durability, highly stable structure, and homogenous atomic distribution produces highly active materials with synergetic catalytic activity and high charge mobility and electron density.

Herein, a portable electrochemical sensor based on the fabrication of interdigitated electrode array (IDA) modified by nitrogen-doped mesoporous carbon spheres (N-doped MCS) and nitrogen-doped carbon hollow trunk (N-doped CHT) was designed. The IDA acted as the portable sensor base that can signal the oxidation–reduction reaction with fast response, low sample volume, and a microfabricated chip. The N-doped CMS and N-doped CHT functionalized the surface of IDA and mediated the detection of NA with high sensitivity and selectivity. The N-doped CMS and M-doped CHT were synthesized using a simple approach, one-pot reaction, and self-assembly management. The surface morphology of the wrinkled and twisted hollow trunk with multiple micrometer-sized open holes, very thin-sided wall, deep penetration, and a cave-like structure facilitated the molecular diffusion and increased the contact interface through the inner/outer surface of N-doped CHT. In addition, the nanoporous network, large surface area, and N-doped graphitic carbon chain ascertained a highly active electrochemical surface that can bind sensitively and selectively to NA targets and rapidly transduce the redox signal. The morphology and chemical composition of N-doped CHT played crucial roles in the fast

response, sensitive and selective assay for NA detection, fast charge transport, facile molecular and electron diffusion, multiple functionalized surfaces, and intense interaction between the surface and target. The N-doped CHT/IDA can be produced for sensitive and selective NA detection in live cells (PC12 cells) with high biocompatibility, high signaling stability, fast response time, low sample volume, and smooth matching with the inner/outer gates in various portable smartphones.

2- Experimental

Electrode design and fabrication of N-doped MCS and N-doped CHT on IDA

2.1 Synthesis of N-doped MCS and N-doped CHT

The N-doped MCS and N-doped CHT-based materials were synthesized based on hydrothermal treatment (HT) approaches of hydrocarbons (i.e., glucose) and other organic compounds at high temperatures [41]. ***For the synthesis of N-doped MCS***, a) a glucose solution (carbon source) was prepared by dissolving 1.8 g glucose (0.2 M) in 30 mL deionized water (DI water), and the mixture was stirred for 2 h. b) The thymine solution (nitrogen atom source) was prepared by dissolving 0.5 g thymine in 0.1 M NaOH (20 mL), sonicated for 1 h and stirring the mixture for 2 h. The solutions of glucose and thymine were mixed and stirred for 1 h at room temperature (solution A).

For the synthesis of N-doped CHT: a) The glucose solution was prepared as described in the previous steps. Sodium dodecyl sulfate (SDS) (0.5 g) was added to the glucose solution. Then, the mixture was sonicated for 30 min and stirred until the formation of a homogeneous solution. The thymine solution was prepared by dissolving 0.5 g in 20 mL 0.1 M NaOH. The glucose and thymine solutions were mixed and then stirred for 2 h (solution B).

Solutions A and B were poured into 100 mL Teflon-sealed autoclaves and maintained at 180 °C for 24 h. After cooling, the black precipitates of N-doped MCS and N-doped CHT were collected. The residues were washed multiple times by a water/ethanol solution (1:1) and then dried at 80 °C for 24 h. The prepared N-doped MCS and N-doped CHT materials

were annealed at 800 °C for 2 h with a step increase in temperature of 3 °C/min under N_2 atmosphere.

2.2 Fabrication of portable sensor based on N-doped MCS and N-doped CHT

A portable sensor was designed based on the modification of the IDA electrode by N-doped MCS and N-doped CHT. The thin films of N-doped MCS and N-doped CHT on the IDA working electrode area were formed by deposition of the ink solutions of these materials using the drop-casting method. The fabrication process was performed as follows: a) The ink solutions of N-doped MCS and N-doped CHT were prepared by diffusing 10 mg of each sample in 1 mL DI water containing 10 µL Nafion solution (5 %wt) (sonication for 2 h). b) The IDA was fabricated by drop-casting 20 µL N-doped MCS and N-doped CHT ink solutions on the open area of the IDA electrode surface. The portable electrodes were named N-doped MCS and N-doped CHT. c) The reference electrode of the IDA electrode was fabricated by the addition of Ag/AgCl ink and heating at 80 °C for 1 min to form a thin-film layer of Ag/AgCl. d) Designed electrode stabilization: Continuous cyclic voltammetry (CV) sweeps in 0.1 M PB (pH = 7) at a scan rate of 100 mVs^{-1} was used to stabilize the IDA working electrodes for 20 cycles within the potential window of 0.0–1.6 V.

3. Results and discussion

3.1 Surface modulation of N-doped MCS and N-doped CHT

Scheme 1 shows the schematic of the synthesis of N-doped MCS and N-doped CHT. The N-doped MCS morphology became self-oriented after HT of glucose and thymine in 0.1 M NaOH solution. The spherical carbon materials formed with variations in size, interlinked spheres, and rough outer surfaces. The controlled formation of carbon materials with a novel morphology was achieved by using SDS as a directing agent. The novel design of N-doped CHT was developed after the removal of SDS by washing several times with ethanol/water solution and carbonization at high temperature, leaving the open trunk-like structure with wrinkled and twisted orientation. During HT, bubbles of CO_2, CO, and H_2

formed and possibly acted as the template for carbon sphere formation [42]. The presence of SDS in the glucose and thymine solutions created hollow spheres that merged to form an open wrinkled and twisted trunk-like structure. The chemical structure of SDS is $CH_3(CH_2)_{11}SO_4Na$ and includes one hydrophilic (sulfate end) and one hydrophobic end (long aliphatic chain end). The hydrophilic end was adsorbed easily at the bubble interface, whereas the hydrophobic end remained inside. The glucose molecules electrostatically adsorbed at the sulfonic group. The adsorbed glucose around the bubbles aromatized and carbonized to form carbon materials of N-doped CHT. The nitrogenous compound of thymine acted as the nitrogen source and electrostatically adsorbed on the bubble surface and SDS molecules. The formed carbon materials interacted with the N source and formed the N-doped carbon-based materials [43-45].

After the removal of SDS by washing and carbonization at high temperature (800 °C under N_2 flow), a novel hollow, twisted, and wrinkled trunk-like structure was formed. A micrometer-sized open hollow with nanometer-sized wall thickness created multiple grooves and vortexes and facilitated molecular and electron diffusion. The surface morphology of N-doped CHT supported the circular diffusion pathway with a high mass-to-volume ratio and induced the high loading of targets on its surface. The N atoms enhanced the characteristic features of the carbon-based materials (linear sp^2 hybridization) by forming multiple functional sites with a high density of electrons and several plane edge defects. The N-doped CHT was produced with a novel geometrical structure of open, hollow, twisted, and wrinkled trunk with multiple micrometer-sized open holes and ultrathin walls and high molecular diffusion through the inner/outer the trunk wall. In addition, the porous structure and high surface area increased the surface interface contact and the loading of targets. Therefore, N-doped CHT can be used as a mediation surface for signaling of ultra-trace concentrations of NA with high sensitivity and selectivity.

Scheme 1

The surface morphology and topography were investigated using field emission-scanning electron microscopy (FE-SEM). Figures 1A(a and b) show the surface morphology and

self-assembly formation of N-doped MCS, respectively. The low-magnification FE-SEM image illustrates the formation of carbon microspheres with various shapes and sizes (Figure 1Aa). The self-assembly of carbon microspheres and thymine in the alkaline medium led to the formation of carbon microspheres with structural defects, such as merged spheres of various sizes (range: 1–2 μm), several of which were egg-like with a round shape. Figure 1Ab shows a focused FE-SEM image indicating the formation of micrometer-sized carbon spheres with surface-to-surface link to the other spheres. In addition, the surface of the spheres was similar to a wave with a rough texture and 3D structure. Figures 1B(a–c) show the energy-dispersive X-ray spectroscopy (EDX)-SEM mapping of N-doped MCS and the atomic distributions of C, O, and N. The homogeneous distributions of C, O, and N reached 20.12, 12.56, and 7.32 %wt, respectively. These data indicate the presence of various functional groups on the surface of N-doped MCS and component N atoms. Figures 1C(a–d) show the FE-SEM images of N-doped CHT and the surface structure design and morphology. A heterogeneous surface was designed based on the direct action of SDS. After the removal of SDS, the final structure of N-doped CHT was formed with high stability. The multiple micrometer-sized open holes in a huge trunk are observed in Figure 1Ca. The holes showed a similar formation of twisted and wrinkled hollow dead tree trunk. The wrinkled and twisted hollow trunk contained numerous surface defects, such as grooves, vortices, and ridges. Figure 1Cb shows the focused FE-SEM image of one of the open holes, which indicates a wrinkled trunk formation with thin walls and multiple holes. The vertical and horizontal cross-section images present the micrometer-sized open holes (hole size: 1–2 μm). The sidewalls of the open holes were extremely thin, with a size of up to 98 nm. The open holes induced interior/exterior molecular diffusion and increased the mass-to volume ratio, leading to a high loading of targets and detection at ultra-low concentrations. Figures 1D(a–d) show the EDX-SEM mapping of N-doped CHT and the homogenous distribution of C (81.83 %wt), O (10.32 %wt), and N (7.85 %wt).

Figure 1

The Raman spectra of carbon materials exhibited carbon formation in the presence of heteroatoms in the carbon chain. Figure 2A shows the Raman shift of N-doped MCS and N-doped CHT. The presence of G (1320 cm^{-1}) and D (1616 cm^{-1}) bands refer to the in-plane vibrational sp^2 hybridization of carbon atoms and the formation of various site defects through the distortion of sp^2 hybridization (sp^3 hybridization), respectively [46-49]. The I_D/I_G values indicate the degree of graphitization and various distorted and plane edge defects. The I_D/I_G values of N-doped MCS and N-doped CHT were 0.94 and 0.97, respectively. Therefore, the N-doped CHT presented a higher graphitization than N-doped MCS, leading to doping of the graphitic carbon chain by N and O atoms (sp^2 hybridization). Figures 2(B and C) show the N_2 adsorption isotherm and nonlocal density functional theory of N-doped MCS (wine line) and N-doped CHT (green line) for the investigation of pore size distribution, surface area, and pore volume. N-doped MCS and N-doped CHT followed a type IV N_2 adsorption isotherm (high step loading at P/P_o = ~0.01). This behavior indicates the dominant mesoporous structure of N-doped MCS and N-doped CHT. The pore size (dp) of N-doped MCS and N-doped CHT was 2.08 nm, with differences in the pore volume (Vp) of 0.042 and 0.083 cm^3g^{-1}, respectively. The large pore volume of mesoporous N-doped CHT, in addition to the open and hollow surface morphology, facilitated the electrolyte diffusion and fast mass transfer inside/outside the designed surface [49, 50]. The wide-angle X-ray diffraction (WA-XRD) indicates the degree of graphitization and conforming distortion of graphitic carbon materials. Figure 2D shows the WA-XRD of N-doped MCS (wine line) and N-doped CHT (green line). Two broad WA-XRD peaks centered at 2Θ = 29.65°, 42° indicate the amorphous graphitic carbon [47]. These data support the existence of heteroatoms and the formation of plane edge defects through the distortion of the graphitic carbon chain due to O and N atoms within the carbon chain (in-plane vibrational sp^2 hybridization) [51]. Figure S1 shows the X-ray photoelectron spectroscopy (XPS) analysis and the presence of C (286.21 eV), O (392.86 eV), and N (532.59 eV) in N-doped CHT. The XPS survey of N1S showed the presence of four peaks centered at 398.21, 299.13, 400.4, and 402.9 eV, representing pyridinic, pyrrolic, quaternary, and graphitic and oxidized N, respectively (Figure 2E) [3,

11, 52]. Nitrogen doping of carbon chain was confirmed by the presence of high contents of pyrrolic and pyridinic N. The redox activity and surface electron charge density were enhanced by pyridinic and pyrrolic N through the carbon chain of N-doped CHT material and improved the sensing property and selectivity toward the NA targets. These characteristics were attained due to the lone electron pair conjugated with the p-coupled rings and the electron support property. Moreover, the electrochemical conductivity and activity were enhanced due to graphitic and oxidized N of the graphitic carbon layers. Figure 2F shows the XPS survey of C1s and the presence of various carbon bond types, including C=C (284.04), C-C (285.75), C=O (288.2), and O-C=C (289.51 eV). Moreover, the XPS survey of O 1S indicated the presence of phenol-type (C–OH), quinone-type (C=O), and groups (C–O–C and C–O–OH), which can provide surface wettability and selectivity to N-doped CHT. Therefore, the surface nature of porosity, high surface area, and formation of N-doped carbon-based materials, in addition to the novel structure of CHT with twisted and wrinkled hollow trunk with multi micrometer-sized open holes, thin-sided walls, deep open holes, rough surface, multi grooves, and vortexes, ascertained the highly active and facile surface for high loading and highly sensitive and selective electrode surface for the detection of target molecules.

Figure 2

3.3 Catalytic activity, sensing property, and selectivity of N-doped MCS/IDA and N-doped CHT/IDA

The catalytic activities of N-doped MCS/IDA, N-doped CHT/IDA, and IDA were tested in $[Fe(CN)_6]^{3-/4-}$ solution (1 mM in 0.1 M KCl) using CV and electrochemical impedance spectroscopy (EIS). Figure 3A shows the CVs of various electrodes of IDA (a), N-doped MCS/IDA (b), and N-doped CHT/IDA (c). The current values (Ia) and applied position difference (ΔE) of the quasi-reversible redox $Fe^{2+/3+}$ peaks were used to outline the catalytic activity and charge transport velocity of the designed electrodes, respectively. The anodic current peak (Ia) values were 3.47, 11.79, and 25.09 μA for IDA, N-doped MCS/IDA, and N-doped CHT/IDA, respectively. The ΔE values were 160 (IDA), 153 (N-doped

MCS/IDA), and 89 (N-doped CHT/IDA) mV. These results indicate the high catalytic activity and fast charge transport of N-doped CHT/IDA. The IDA, N-doped MCS/IDA, and N-doped CHT/IDA electrode surface areas were calculated from the Randles–Sevick formula: [53]

$$Ia\ (A) = 2.69 \times 10^5\ n^{3/2}\ A_0 D_0^{1/2} C_0 \nu^{1/2} \quad (1)$$

where Ia (A) refers to the anodic peak current, n represents the number of electrons transferred, D ($cm^2\ s^{-1}$) is the diffusion coefficient, C_0 (mole cm^{-3}) is the $[K_3Fe(CN)_6]$ concentration, A (cm^2) is the electrode surface area, and ν ($V\ s^{-1}$) is the scan rate [54]. The calculated electrode surface areas were 0.0013, 0.005, and 0.01 cm^2 for IDA, N-doped MCS/IDA, and N-doped CHT/IDA, respectively. The N-doped CHT/IDA exhibited a higher electrode surface area than N-doped MCS/IDA (twofold) and IDA (10-fold). Therefore, N-doped CHT/IDA showed the best catalytic activity and highest surface-to-volume ratio with fast charge mobility and facile electron diffusion.

Figure 3B shows the EIS Nyquist plot of IDA (a), N-doped MCS/ID (b), and N-doped CHT/IDA (c). The semicircle at high frequency signifies the surface charge resistance (Ret), whereas the line pathway at low frequency signifies electron diffusion on the electrode surface. The inset in Figure 3 illustrates the lowest semicircle and highest line pathway of N-doped CHT/IDA compared with IDA and N-doped MCS/IDA. These results denote the fast charge transport and low surface resistance of N-doped CHT/IDA, leading to the design of a highly active electrode surface for sensing and biosensing applications.

The sensing property of various electrodes (IDA, N-doped MCS/IDA, and N-doped CHT/IDA) for the detection of NA was studied using CV on PB (pH = 7) containing 100 µM NA at a scan rate of 100 mVs^{-1} and in the range of –0.2 V to 0.8 V· Figure 3C shows the CVs of IDA (a), N-doped MCS/IDA (b), and N-doped CHT/IDA (c). Four well-known peaks were observed for the oxidation–reduction of NA with the applied potential difference of 76 mV, indicating that the oxidation–reduction of NA is quasi-reversible process [11, 26-28, 61]. The NA was oxidized to o-quinone with losing of $2e^-/2H^{+}$· The N-doped CHT/IDA presented the highest and sharpest peaks for NA compared with other electrodes of IDA and N-doped MCS/IDA. This result may be related to the novel

geometric structure of open trunks similar to a heart, micrometer-sized holes, thin hole edges (70–100 nm), surface heterogeneity orientation of inner/outer free spaces with high Brunauer–Emmett–Teller (BET) surface area, mesoporous network, and high electrode surface area. Further confirming the sensing property of N-doped CHT/IDA, various NA concentrations (0, 100, and 200 µM) were measured using CV (Figure 3D). With the increased concentrations of NA, the corresponding peak current increased. Therefore, the N-doped CHT/IDA was used as an active portable sensor for NA detection.

Figure 3

3.4 Physicochemical parameters for sensing performance and surface interaction of NA on N-doped CHT/IDA

Physicochemical parameters, including pH and surface interaction, that influence the sensing property were used to understand the surface–target interaction. The pH dependence of the supporting electrolyte was studied using CV of N-doped CHT/IDA. Figure S2A shows the CVs of 100 µM NA under various pH (5.2 to 8) within the scan rate of 100 mVs^{-1}. The peak position (E) and anodic (Ia) and cathodic (Ic) current peak values varied as the pH changed. A high current value was observed at pH = 7. Thus, this pH was considered the optimum and near the physiological value (Figure S2B). pH and E/V exhibited a linear relationship with a regression equation of E(V) = 0.63 – 0.059 pH, R^2 = 0.995 (Figure S2C). This result indicates the proton participation in the overall NA electrooxidation and followed the mechanism of losing and accepting $2e^-/2H^+$ (slope = 59 mV, which equals the theoretical Nernst value) [21, 41, 55].

The controlled interaction of N-doped CHT/IDA surface to NA molecules was investigated using the scan rate effect (20–280 mVs^{-1}). Figure S2D shows the CVs of 100 µM NA under varied scan rates. The Ia and Ic peak values increased as the scan rate increased (Figure S2E). The relationships between the plot of scan rate versus the Ia and Ic were linear with the regression equations of Ia (µA) = 9 + 0.21 ν (mVs^{-1}), R^2 = 0.994 and Ic (µA) = 0.87 – 0.1 ν (mVs^{-1}), R^2 = 0.997 (S/N = 3), respectively. Moreover, the applied potential varied with the scan rate function, indicating that the adsorption-controlled process is the actual NA mechanism on the surface of N-doped CHT/IDA [41, 56].

By applying the following equation, the adsorbed NA molecules (Γ) on the surface of N-doped CHT/IDA was calculated to be 5.59 nM cm^{-2} [57]:

$$I_a = n^2F^2\Gamma\nu A/4RT, \quad (1)$$

where A is the IDA surface area, n is the number of electrons transferred, T is the absolute temperature, F is Faraday's constant, R is the gas constant, and ν is the scan rate.

The physical parameters of the electrode interaction of NA to N-doped CHT/IDA surface (charge transfer coefficient (α) and electron transfer rate constant (Ks)) were estimated. Figure S2F shows the plot of Ea and Ec versus ln ν. The linear relationships were accompanied with regression equations of Ea (V) = 0.29 + 72×10^{-5} lnv (V s^{-1}) (R^2 = 0.965) and Ec(V) = 0.211 - 87×10^{-5} log v (V s^{-1}) (R^2 = 0.92).

By applying Laviron's theory [58], the following equation was obtained:

$$\log k_a/k_c = \log \alpha/(1-\alpha) \text{ or } k_a/k_c = \alpha/(1-\alpha) \quad (2)$$

where Ka (slope of Ea vs. log ν) equals 2.3RT/ (1 − α) nF, and Kc (the slope of Ec vs. log ν) equals −2.3RT/αnF. The calculated values of α and Ks were 0.525 s and 0.21 cms^{-1}, respectively.

3.4 Sensitivity, stability, and reproducibility of the portable N-doped CHT/IDA

A portable sensor was designed based on an IDA covered by N-doped CHT/IDA for signaling NA level in human neuronal cell lines. The sensitivity, stability, linear range, detection limit, and calibration curve of the N-doped CHT/IDA-based sensor were investigated using square wave voltammetry (SWV) and chronoamperometry (CA). The SWVs of various NA concentrations ranged from 0.01 µM to 0.3 µM, implying the design of a highly sensitive portable NA sensor based on N-doped CHT/IDA (Figure Aa). The SWV peak current increased with the dynamic and dramatic increase in NA concentrations. The calibration curve of the plot of NA concentrations (µM) versus current (µA) showed a wide linear relationship (0.01–0.3 µM) with the regression equation of I (µA) = 9.7 + 17.7 [NA](µM), R^2 = 0.997 (S/N = 3) (Figure 4Ab). The calculated detection limit was 0.005

μM with a high sensitivity of 1770 μA/μM×cm^2. The detection limit of the portable NA sensor was calculated from the calibration curve (Figure 4Ab), according to the following equation of 3σ/n; where σ is the standard error of the intercept and n is the slope value.

The sensitivity and stability of the portable N-doped CHT/IDA sensor were evident within a wide range of concentrations at fixed applied potentials, as evidenced from the CA analysis (Figure 4Ba). Figure 4Ba shows the CA response of various NA concentrations (0.01–2 μM) injected into the PB (pH = 7) under continuous stirring, N2 flow, and fixed applied potential of 0.27 V. The stable and step increase of the CA current as a function of various NA concentration groups (10, 25, 50, 100, and 500 nM) verified the high sensitivity and stability of the portable electrode of N-doped CHT/IDA. The calibration plot of the wide concentration range of 0.01–2 μM versus the current showed good linear behavior and low detection limit of 90 nM with the regression equation of Ia (μA) = 0.9 + 11.3 [NA](μM), R^2 = 0.963 (S/N = 3) (Figure 4Bb). Figure 4Bc shows the detection of ultra-low concentration of NA (0.01–0.1 μM) by CA. The calibration plot within the range of 0.01–0.1 μM showed a linear relationship and a low detection limit of 0.006 μM with high sensitivity of 320 μA/μM×cm^2. These results support the highly sensitive NA portable sensor design based on N-doped CHT/IDA resulting from the surface morphology (micrometer-sized open holes, thin walls, interlinked open trunks, high surface area, and mesoporous network) and chemical composition (N-doped carbon chain that produced multifunctional active sites and induced the electrochemical conductivity). The N-doped CHT/IDA acted as an ultra-low-concentration detective sensor compared with the other designed electrodes (Table 1). Comparison of different electrodes and N-doped CHT/IDA (i.e., based on the detection limit and linear DA detection range) indicate the opportunities for fast-detection, high-stability, high-economy, and on-site detection by portable NA sensors with low sample volume and high sensitivity and selectivity.

Figure 4

The selectivity of N-doped CHT/IDA was studied using CV and SWV techniques in the presence of various competitive interfering molecules. For example, it is well-known that ascorbic acid (AA) and uric acid (UA) are potential interfering molecules of NA detection [23, 53]. Figure S3A shows the CVs of 500 µM AA and 100 µM NA on N-doped CHT/IDA. Two well defined peaks were observed at applied potentials of 0.123 and 0.27 V for AA and NA, respectively. The selectivity of N-doped CHT/IDA was confirmed by screening the interfering molecules in one-pot method (AA and UA). As presented in Figure S3B, three well-defined CV peaks were observed for AA, NA, and UA at applied potentials of 0.126, 0.27, and 0.4 V, respectively. The peak-to-peak potential separation of AA–NA (0.144 V), AA–UA (0.274 V), and NA–UA (0.13 V) confirmed the design of NA-selective sensor based on N-doped CHT/IDA. Furthermore, Figure S3C shows the SWV measurements of 1 µM NA only (red line), and 1 µM NA in the presence of 1 µM dopamine (DA), 1 µM epinephrine (EP), 500 µM AA, 1000 µM glucose (Gl), and 100 1 µM UA. By plotting of the current value of NA (19.89 µA) as compared to the current response of the other molecules, a strong and high current value have been observed for NA. Our finding shows that low current values for DA (1.53 µA) and EP (2.31 µA) are observed. Meanwhile, no significant current responses for Gl, AA, and UA molecules were evident. This result indicates that the N-doped CHT/IDA electrode-based material is sensitive and selective NA portable sensor design.

Overall, the results showed real evidence that the N-doped CHT/IDA portable sensor featured certain advantages; i) strong signaling of NA in the presence of various interfering molecules, ii) low sample volume and sensitive NA response, and iii) highly stable and reproducible response upon the stable and dramatic increase of the anodic and catholic peak current at a fixed applied potential (0.27 V). The key parameters of our portable electrode-based materials such as i) high BET surface area, ii) novel open trunk morphology similar to that of a heart, including micrometer-sized holes, thin walls, and high surface-to-volume ratio, iii) porous structure, iv) N-doped graphitic carbon chain that creates a multifunctional surface with high electron density, v) several active sites with numerous plane edge defects,

vi) strong binding to NA targets, and vii) fast charge transport with low surface resistance play significant role in the leverage NA sensing system [11, 30, 34, 38].

The stability and reproducibility of the devices were investigated by CA using different samples and portable electrodes to detect NA. Figure S4A shows a stable and sensitive CA response for the detection of NA (0.1 µM). The calculated relative standard deviation (%RSD) of 2.9 and a standard deviation (SDEV) of ±0.015 µM (Figure S4A). A reproducible device was optimized after designing 5 electrodes and measuring 0.25 µM NA by CA. A stable response was observed with %RSD = 2.6 and SDEV= ±0.039 µM (Figure S4C). The highly stable and reproducible device based on N-doped CHT/IDA showed good applicability and portability for measuring NA in its resources and receptors. Figures S4 (E&F) show the SEM-images N-doped CHT at the electrode substrate surface of IDA. The designed electrode surface is highly stable and shows a homogeneous and open hollow trunk design that facilitates the diffusion of NA-electrolytes outward/downward the electrode. These data provide the surface dependent of N-doped CHT/IDA for designing of highly active NA-sensor with high sensitivity and stability.

Table 1. Survey of NA detections using different modified electrodes obtaining the limit of detection and linear range for each one, and the detection limit of N-doped CHT/IDA with its linear range.

Electrode	Limit of detection (µM)	Linear range (µM)	Ref.
S-CSN-1[1]	0.001	0.01– 0.8	[7]
CNNB-1[2]	0.009	0.5 – 32	[11]
fMWCNT/GCE[3]	0.0043	0.7 – 100	[25]
ZnO/CNTs	0.02	0.05 - 4500	[27]
5ADBCN/ PE[4]	0.6	1.2 – 900	[29]
CNT-molybdenum (VI) complex (MC)/PE	0.043	30 – 700	[59]
Hematoxylin/GCE	0.09	0.7 – 2000	[60]
P-trypan blue/GCE	0.06	0.1 – 560	[61]
CNT/PE[5]	0.21	0.47 – 5000	[62]
GC/MWCNT/FCo98 [6]	0.76	160 – 1910	[63]
SiTi/AuNP	0.35		[64]
Activated pencil graphite electrode	0. 832	2.5 – 250	[65]
MoO_3 NWs/GCE	0.11	0.1 - 2000	[66]
N-doped CHT	0.005	0.01 – 0.3	This work

[1]Sulfur-doped carbon spheroidal surface
[2]CNNB-1: C-, N doped NiO broccoli-like hierarchy
[3]fMWCNT: flavonoid multiwall carbon nanotube
[4]5ADBCN; 5-mino-3′,4′- dimethyl-biphenyl-2-ol (5ADB)
[5]CNT; carbon nanotube PE: paste electrode
[6] Cobalt ferrite nanoparticles and carbon nanotubes

3.7 Sensitivity assay for monitoring of DA in dopaminergic cells (PC12)

Early and proper diagnosis will help in minimizing sickness, thereby reducing healthcare costs. The levels of monoamine neurotransmitters such as NA are abnormally low in the human brain [67, 68]. The N-doped CHT/IDA was designed for in-vitro monitoring of NA released from PC12 cells (neuronal cell line model), conveying the portable sensor's benefits, including the low sample volume, easy fabrication, and on-site detection.

The biocompatibility and cytotoxicity of N-doped CHT were investigated using confocal microscopy and Cell Counting Kit (CCK)-8 cytotoxicity assay. Figures 5A–D show the confocal microscopy images of PC12 cells incubated with 100 mg/mL N-doped CHT. Figure 5A displays the bright-field image of N-doped CHT and PC12 cells and confirms the presence of studied the materials around the cells. The PC12 structural morphology (cytoskeleton) and nucleus were unaffected by the presence of N-doped CHT (Figures 5B and 5C, respectively). Figure 5D shows the merged images of the nucleus (4′,6-diamidino-2-phenylindole (DAPI) counterstaining) and F-actine (phalloidin 488) staining fluorescence of PC12 cells. These data illustrate that the N-doped CHT is biocompatible due to its stable structure, and no damages were observed on the PC12 cell structure. The CCK-8 assay protocol was used to study the cytotoxicity of N-doped CHT to PC12 cells. Various N-doped CHT concentrations (20–250 µg/mL) were incubated with PC12 cells (1×10^6 cells/mL). Figure 5E shows the column plot of N-doped CHT concentrations (µg/mL) versus the % viability. At 50 µg/mL concentration, 98.4% of the cells were viable, whereas at high concentrations (250 µg/mL), 83.2% of the cells were alive. Therefore, N-doped CHT showed low cytotoxicity to the PC12 cells, indicating its high biocompatibility and applicability for in-vitro and in-vivo applications. A portable sensor design based on N-doped CHT/IDA was fabricated for in-vitro monitoring of NA released from PC12 cells. The N-doped CHT/IDA was tested to measure the NA secreted from PC12 cells by changing the stimulating agent concentrations (0–50 mM KCl) using SWV measurements. Figure 5F shows the column plot of [KCl]/(mM) versus the response current of the cell's supernatant. With the increase in K^+ concentrations, the anodic current response increased. The exact functions of potassium ions occurred on the cell membrane and included the

depolarization and opening up of voltage-gated Na^+ and Ca^{2+} channels [69]. Scheme 2 shows the design of a highly sensitive portable NA sensor based on N-doped CHT/IDA. Furthermore, N-doped CHT/IDA may be employed in therapeutic applications and early-stage diagnostics of certain neurological conditions such as Alzheimer's disease. The portable sensor using N-doped CHT/IDA offers sensitivity, selectivity, low cytotoxicity, and high biocompatibility for NA monitoring in live cells.

Figure 5

Scheme 2

Conclusion

In-vitro monitoring of neurotransmitters (i.e., NA) is regarded as a biomarker for the follow-up of several neuronal disorders, such as Alzheimer's, schizophrenia, and Parkinson's disease. This work focused on the design of a portable sensor for the in-vitro detection of NA released from live cells (PC12). The portable NA sensor was designed based on the functionalization of chipset IDA using N-doped carbon materials. N-doped MCS and N-doped CHT materials were used to modify the IDA after the controlled formation of a thin-film layer on the working area. The sensing property and electrochemical activity were studied using CV and EIS and indicated the high catalytic activity and sensing property of N-doped CHT. The controlled design of a hollow trunk (N-doped CHT)-like structure included multiple holes in various positions, deep hole penetration, thin-sided walls, wrinkled and twisted surface formation, and numerous free spaces through holes and pores. The N atom components doped on the graphitic carbon chain induced the surface functionality and charge transport velocity with a highly charged surface, numerous plane edge defects, and a pool of electrons. The structure and chemical composition features of N-doped CHT illustrate a highly active mediator with facile molecular/electron diffusion through the inner/outer surface, fast charge transport, strong binding to NA targets, and high loading of targets. The N-doped CHT showed high biocompatibility and low cytotoxicity and matched well with the DAPI nucleus counterstaining, indicating the applicability of the sensor for the detection of NA secreted during in-vitro monitoring of PC12 cells. The portable N-doped CHT sensor showed a high

selectivity for NA with a high sensitivity of 1770 μA/μM×cm^2, a low detection limit of 0.005 μM, and a wide linear range of 0.01–0.3 μM. A portable N-doped CHT/IDA sensor was designed for the in-vitro monitoring of NA secreted from live cells, and it exhibited high sensitivity and selectivity, facile signaling stability, good stability, high biocompatibility, and good reproducibility. The N-doped CHT/IDA was applied as a portable NA sensor for live cells. This sensor can be used for on-site detection and daily monitoring of various neuronal diseases and advance the use of portable healthcare devices.

Acknowledgment

This work was supported by the Japan Society for the Promotion of Science (JSPS), grant No. P19067.

Declarations

The authors declare that there is no conflect of interest

References

[1] V. Hefco, K. Yamada, A. Hefco, L. Hritcu, A. Tiron, T. Nabeshima, Role of the mesotelencephalic dopamine system in learning and memory processes in the rat, Eur. J. Pharm., 475 (2003) 55-60.

[2] A.S. Moody, B. Sharma, Multi-metal, multi-wavelength surface-enhanced raman spectroscopy detection of neurotransmitters, ACS Chem. Neurosc., 9 (2018) 1380-1387.

[3] M.Y. Emran, H. Khalifa, H. Gomaa, M.A. Shenashen, N. Akhtar, M. Mekawy, A. Faheem, S.A. El-Safty, Hierarchical CN doped NiO with dual-head echinop flowers for ultrasensitive monitoring of epinephrine in human blood serum, Microchim. Acta, 184 (2017) 4553-4562.

[4] W.G. Meijer, S.C. Copray, H. Hollema, I.P. Kema, N. Zwart, I. Mantingh-Otter, T.P. Links, P.H. Willemse, E.G. de Vries, Catecholamine-synthesizing enzymes in carcinoid tumors and pheochromocytomas, Clin. Chem., 49 (2003) 586-593.

[5] D.L. Wong, Epinephrine biosynthesis: hormonal and neural control during stress, Cell. Molec. Neurobiol., 26 (2006) 889-898.

[6] F. Lechin, B. Van Der Dijs, A.E. Lechin, Circulating serotonin, catecholamines, and central nervous system circuitry related to some cardiorespiratory, vascular, and hematological disorders, J. Appl.Res., 5 (2005) 605-621.

[7] M.Y. Emran, M.A. Shenashen, S.A. El-Safty, M.M. Selim, T. Minowa, A. Elmarakbi, Three-Dimensional Circular Surface Curvature of a Spherule-Based Electrode for Selective Signaling and Dynamic Mobility of Norepinephrine in Living Cells, ACS Appl. Bio Mater., 3 (2020), 8496-8506.

[8] M. Ciccarelli, D. Sorriento, E. Coscioni, G. Iaccarino, G. Santulli, Adrenergic receptors, Endocrinology of the Heart in Health and Disease, Elsevier2017, pp. 285-315.

[9] I. Cova, A. Priori, Diagnostic biomarkers for Parkinson's disease at a glance: where are we?, J. Neural Transm., 125 (2018) 1417-1432.

[10] R. Cerroni, C. Liguori, A. Stefani, M. Conti, E. Garasto, M. Pierantozzi, N.B. Mercuri, S. Bernardini, G. Fucci, R. Massoud, Increased Noradrenaline as an Additional

Cerebrospinal Fluid Biomarker in PSP-Like Parkinsonism, Front. Aging Neurosc., 12 (2020) 126.
[11] M.Y. Emran, M. Mekawy, N. Akhtar, M.A. Shenashen, I.M. EL-Sewify, A. Faheem, S.A. El-Safty, Broccoli-shaped biosensor hierarchy for electrochemical screening of noradrenaline in living cells, Biosens. Bioelectron., 100 (2018) 122-131.
[12] S. Terbeck, J. Savulescu, L. Chesterman, P. Cowen, Noradrenaline effects on social behaviour, intergroup relations, and moral decisions, Neurosc. Biobehav. Rev., 66 (2016) 54-60.
[13] G. Eisenhofer, K. Pacak, T.-T. Huynh, N. Qin, G. Bratslavsky, W.M. Linehan, M. Mannelli, P. Friberg, H.J. Timmers, S.R. Bornstein, Catecholamine metabolomic and secretory phenotypes in phaeochromocytoma, Endocrine-related cancer, 18 (2011) 97.
[14] S. Casadio, J. Lowdon, K. Betlem, J. Ueta, C.W. Foster, T. Cleij, B. van Grinsven, O. Sutcliffe, C.E. Banks, M. Peeters, Development of a novel flexible polymer-based biosensor platform for the thermal detection of noradrenaline in aqueous solutions, Chem. Eng. J., 315 (2017) 459-468.
[15] F. Robert, L. Bert, L. Lambás-Señas, L. Denoroy, B. Renaud, In vivo monitoring of extracellular noradrenaline and glutamate from rat brain cortex with 2-min microdialysis sampling using capillary electrophoresis with laser-induced fluorescence detection, J. Neurosc. Meth., 70 (1996) 153-162.
[16] Q. Zhou, S.-Z. Kang, X. Li, L. Wang, L. Qin, J. Mu, One-pot hydrothermal preparation of wurtzite CuGaS2 and its application as a photoluminescent probe for trace detection of l-noradrenaline, Coll. Surf. A: Physicochem. Eng. Asp., 465 (2015) 124-129.
[17] L. Zhang, X.A. Liu, K.D. Gillis, T.E. Glass, A High-Affinity Fluorescent Sensor for Catecholamine: Application to Monitoring Norepinephrine Exocytosis, Ang. Chem. Int. Ed., 58 (2019) 7611-7614.
[18] M. Jian, H. Huang, K. Li, L. Chuan, L. Li, L. Jiang, A 3-min UPLC-MS/MS method for the simultaneous determination of plasma catecholamines and their metabolites: Method verification and diagnostic efficiency, Clin. Biochem., 87 (2021) 67-73.

[19] M. Buleandră, D.E. Popa, I.G. David, A.A. Ciucu, A simple and efficient cyclic square wave voltammetric method for simultaneous determination of epinephrine and norepinephrine using an activated pencil graphite electrode, Microchem. J., 160 (2021) 105621.
[20] K.-D. Seo, M.M. Hossain, N. Gurudatt, C.S. Choi, M.J. Shiddiky, D.-S. Park, Y.-B. Shim, Microfluidic neurotransmitters sensor in blood plasma with mediator-immobilized conducting polymer/N, S-doped porous carbon composite, Sens. Actuat. B: Chem., 313 (2020) 128017.
[21] M.Y. Emran, S.A. El-Safty, M.M. Selim, T. Minowa, A. Elmarakbi, M.A. Shenashen, Non-metal sensory electrode design and protocol of DNA-nucleobases in living cells exposed to oxidative stresses, Anal. Chim. Acta, 1142 (2021) 143-156.
[22] A.A. Abdelwahab, A.H. Naggar, M. Abdelmotaleb, M.Y. Emran, Ruthenium Nanoparticles Uniformly-designed Chemically Treated Graphene Oxide Nanosheets for Simultaneous Voltammetric Determination of Dopamine and Acetaminophen, Electroanalysis, 32 (2020) 2156-2165.
[23] M.Y. Emran, M.A. Shenashen, A. El Sabagh, M.M. Selim, S.A. El-Safty, Enzymeless copper microspheres@carbon sensor design for sensitive and selective acetylcholine screening in human serum, Coll. Surf. B: Biointerf., 210 (2022) 112228.
[24] J.-M. Moon, N. Thapliyal, K.K. Hussain, R.N. Goyal, Y.-B. Shim, Conducting polymer-based electrochemical biosensors for neurotransmitters: A review, Biosens. Bioelectron., 102 (2018) 540-552.
[25] M. Amiri-Aref, J.B. Raoof, R. Ojani, A highly sensitive electrochemical sensor for simultaneous voltammetric determination of noradrenaline, acetaminophen, xanthine and caffeine based on a flavonoid nanostructured modified glassy carbon electrode, Sens. Actuat. B: Chem., 192 (2014) 634-641.
[26] H. Devnani, S.P. Satsangee, R. Jain, Nanocomposite modified electrochemical sensor for sensitive and selective determination of noradrenaline, Mater. Tod.: Proceed., 3 (2016) 1854-1863.

[27] A. Pahlavan, V.K. Gupta, A.L. Sanati, F. Karimi, M. Yoosefian, M. Ghadami, ZnO/CNTs nanocomposite/ionic liquid carbon paste electrode for determination of noradrenaline in human samples, Electrochim. Acta, 123 (2014) 456-462.

[28] M.Y. Emran, M.A. Shenashen, A.I. Eid, M.M. Selim, S.A. El-Safty, Portable sensitive and selective biosensing assay of dopamine in live cells using dual phosphorus and nitrogen doped carbon urchin-like structure, Chem. Eng. J. (2021) 132818. https://doi.org/10.1016/j.cej.2021.132818

[29] H. Beitollahi, S. Mohammadi, Selective voltammetric determination of norepinephrine in the presence of acetaminophen and tryptophan on the surface of a modified carbon nanotube paste electrode, Mater.Sci. Eng. C, 33 (2013) 3214-3219.

[30] M.A. Shenashen, M.Y. Emran, A. El Sabagh, M.M. Selim, A. Elmarakbi, S.A. El-Safty, Progress in sensory devices of pesticides, pathogens, coronavirus, and chemical additives and hazards in food assessment: Food safety concerns, Prog. Mater.Sci., 124 (2022) 100866.

[31] S. Murugesan, T. Scheibel, Copolymer/Clay Nanocomposites for Biomedical Applications, Adv. Funct. Mater., 30 (2020) 1908101.

[32] X. Hu, M. Fan, Y. Zhu, Q. Zhu, Q. Song, Z. Dong, Biomass-derived phosphorus-doped carbon materials as efficient metal-free catalysts for selective aerobic oxidation of alcohols, Green Chem. 21 (2019) 5274-5283.

[33] M.Y. Emran, M.A. Shenashen, S.A. El-Safty, M.M. Selim, Design of porous S-doped carbon nanostructured electrode sensor for sensitive and selective detection of guanine from DNA samples, Microp. Mesop. Mater., 320 (2021) 111097.

[34] J. Wu, C. Jin, Z. Yang, J. Tian, R. Yang, Synthesis of phosphorus-doped carbon hollow spheres as efficient metal-free electrocatalysts for oxygen reduction, Carbon, 82 (2015) 562-571.

[35] D. Wang, N.B. Saleh, W. Sun, C.M. Park, C. Shen, N. Aich, W.J. Peijnenburg, W. Zhang, Y. Jin, C. Su, Next-generation multifunctional carbon–metal nanohybrids for energy and environmental applications, Env. Sci. Tech., 53 (2019) 7265-7287.

[36] Y.N. Sun, M.L. Zhang, L. Zhao, Z.Y. Sui, Z.Y. Sun, B.H. Han, AN, P Dual-Doped Carbon with High Porosity as an Advanced Metal-Free Oxygen Reduction Catalyst, Adv. Mater. Interfaces, 6 (2019) 1900592.

[37] M.Y. Emran, S.A. El-Safty, M.M. Selim, M.A. Shenashen, Selective monitoring of ultra-trace guanine and adenine from hydrolyzed DNA using boron-doped carbon electrode surfaces, Sens.Actuat. B: Chem., 329 (2021) 129192.

[38] M.Y. Emran, M.A. Shenashen, S.A. El-Safty, A. Reda, M.M. Selim, Microporous P-doped carbon spheres sensory electrode for voltammetry and amperometry adrenaline screening in human fluids, Microchim. Acta, 188 (2021) 1-11.

[39] J. Li, J. Jiang, H. Feng, Z. Xu, S. Tang, P. Deng, D. Qian, Facile synthesis of 3D porous nitrogen-doped graphene as an efficient electrocatalyst for adenine sensing, RSC Adv., 6 (2016) 31565-31573.

[40] M.Y. Emran, S.A. El-Safty, A. Elmarakbi, A. Reda, A. El Sabagh, M.A. Shenashen, Chipset Nanosensor Based on N-Doped Carbon Nanobuds for Selective Screening of Epinephrine in Human Samples, Adv.Mater. Interfces, (2021) 2101473. https://doi.org/10.1002/admi.202101473

[41] M.Y. Emran, M.A. Shenashen, A.A. Abdelwahab, M. Abdelmottaleb, S.A. El-Safty, Facile synthesis of microporous sulfur-doped carbon spheres as electrodes for ultrasensitive detection of ascorbic acid in food and pharmaceutical products, New J. Chem. 42 (2018) 5037-5044.

[42] Y. Qu, Z. Zhang, X. Wang, Y. Lai, Y. Liu, J. Li, A simple SDS-assisted self-assembly method for the synthesis of hollow carbon nanospheres to encapsulate sulfur for advanced lithium–sulfur batteries, J. Mater. Chem. A, 1 (2013) 14306-14310.

[43] Q. Peng, Y. Dong, Y. Li, ZnSe semiconductor hollow microspheres, Ang.Chemie Int. Ed., 42 (2003) 3027-3030.

[44] H.B. de Aguiar, M.L. Strader, A.G.F. de Beer, S. Roke, Surface Structure of Sodium Dodecyl Sulfate Surfactant and Oil at the Oil-in-Water Droplet Liquid/Liquid Interface: A Manifestation of a Nonequilibrium Surface State, J. Phy. Chem. B, 115 (2011) 2970-2978.

[45] S. Li, A. Pasc, V. Fierro, A. Celzard, Hollow carbon spheres, synthesis and applications–a review, J. Mater. Chem. A, 4 (2016) 12686-12713.
[46] Y. Sun, J. Wu, J. Tian, C. Jin, R. Yang, Sulfur-doped carbon spheres as efficient metal-free electrocatalysts for oxygen reduction reaction, Electrochim. Acta, 178 (2015) 806-812.
[47] W. Chaikittisilp, M. Hu, H. Wang, H.-S. Huang, T. Fujita, K.C.-W. Wu, L.-C. Chen, Y. Yamauchi, K. Ariga, Nanoporous carbons through direct carbonization of a zeolitic imidazolate framework for supercapacitor electrodes, Chem. Commun., 48 (2012) 7259-7261.
[48] H.T. Kim, H. Shin, I.Y. Jeon, M. Yousaf, J. Baik, H.W. Cheong, N. Park, J.B. Baek, T.H. Kwon, Carbon–Heteroatom Bond Formation by an Ultrasonic Chemical Reaction for Energy Storage Systems, Adv. Mater., 29 (2017) 1702747.
[49] Z. Chen, M. Zhang, Y. Wang, Z. Yang, D. Hu, Y. Tang, K. Yan, Controllable synthesis of nitrogen-doped porous carbon from metal-polluted miscanthus waste boosting for supercapacitors, Green Energy Env., 6 (2021) 929-937.
[50] Q. Wang, Y. Zhou, X. Zhao, K. Chen, G. Bingni, T. Yang, H. Zhang, W. Yang, J. Chen, Tailoring carbon nanomaterials via a molecular scissor, Nano Tod., 36 (2021) 101033.
[51] M.A. Moyad, M.A. Combs, D.C. Crowley, J.E. Baisley, P. Sharma, A.S. Vrablic, M. Evans, Vitamin C with metabolites reduce oxalate levels compared to ascorbic acid: a preliminary and novel clinical urologic finding, Urol Nurs, 29 (2009) 95-102.
[52] Z. Li, F. Bu, J. Wei, W. Yao, L. Wang, Z. Chen, D. Pan, M. Wu, Boosting the energy storage densities of supercapacitors by incorporating N-doped graphene quantum dots into cubic porous carbon, Nanoscale, 10 (2018) 22871-22883.
[53] D. Buttry, A. Bard, Electroanalytical chemistry, vol. 17, New York: Marcel Dekker, 1991.
[54] P. Zuman, Z. Fijalek, Contribution to the understanding of the reduction mechanism of nitrobenzene, J. Electroanal. Chem. Interfacial Electrochem., 296 (1990) 583-588.

[55] M.Y. Emran, S.A. El-Safty, M.M. Selim, A. Reda, H. Morita, M.A. Shenashen, Electrochemical sensors-based phosphorus-doped carbon for determination of adenine DNA-nucleobases in living cells, Carbon, 173 (2021) 1093-1104.
[56] M.Y. Emran, E. Talat, S.A. El-Safty, M.A. Shenashen, E.M. Saad, Influence of hollow sphere surface heterogeneity and geometry of N-doped carbon on sensitive monitoring of acetaminophen in human fluids and pharmaceutical products, New J. Chem., 45 (2021) 5452-5462.
[57] M. Sharp, M. Petersson, K. Edström, Preliminary determinations of electron transfer kinetics involving ferrocene covalently attached to a platinum surface, J. Electroanal. Chem. Interfacial Electrochem., 95 (1979) 123-130.
[58] E. Laviron, General expression of the linear potential sweep voltammogram in the case of diffusionless electrochemical systems, J. Electroanal. Chem. Interfacial Electrochem., 101 (1979) 19-28.
[59] H. Beitollahi, I. Sheikhshoaie, Selective voltammetric determination of norepinephrine in the presence of acetaminophen and folic acid at a modified carbon nanotube paste electrode, J. Electroanal.Chem., 661 (2011) 336-342.
[60] N. Nasirizadeh, H.R. Zare, Differential pulse voltammetric simultaneous determination of noradrenalin and acetaminophen using a hematoxylin biosensor, Talanta, 80 (2009) 656-663.
[61] M. Taei, M.S. Jamshidi, A voltammetric sensor for simultaneous determination of ascorbic acid, noradrenaline, acetaminophen and tryptophan, Microchem. J., 130 (2017) 108-115.
[62] M.R. Akhgar, H. Beitollahi, M. Salari, H. Karimi-Maleh, H. Zamani, Fabrication of a sensor for simultaneous determination of norepinephrine, acetaminophen and tryptophan using a modified carbon nanotube paste electrode, Anal. Meth., 4 (2012) 259-264.
[63] D.F.d. Queiroz, T.R.d.L. Dadamos, S.A.S. Machado, M.A.U. Martines, Electrochemical Determination of Norepinephrine by Means of Modified Glassy Carbon Electrodes with Carbon Nanotubes and Magnetic Nanoparticles of Cobalt Ferrite, Sensors (Basel), 18 (2018) 1223.

[64] F.d.M. Morawski, B.B. Xavier, A.H. Virgili, K.d.S. Caetano, E.W. de Menezes, E.V. Benvenutti, T.M.H. Costa, L.T. Arenas, A novel electrochemical platform based on mesoporous silica/titania and gold nanoparticles for simultaneous determination of norepinephrine and dopamine, Mater. Sci. Eng. C, 120 (2021) 111646.
[65] M. Buleandră, D.E. Popa, I.G. David, A.A. Ciucu, A simple and efficient cyclic square wave voltammetric method for simultaneous determination of epinephrine and norepinephrine using an activated pencil graphite electrode, Microchem. J., 160 (2021) 105621.
[66] K.J. Samdani, D.W. Joh, M.K. Rath, K.T. Lee, Electrochemical mediatorless detection of norepinephrine based on MoO3 nanowires, Electrochim.Acta, 252 (2017) 268-274.
[67] Y. Liu, X. He, P. Ma, Y. Huang, X. Li, Y. Sun, X. Wang, D. Song, Fluorometric detection of dopamine based on 3-aminophenylboronic acid-functionalized AgInZnS QDs and cells imaging, Talanta, 217 (2020) 121081.
[68] S.T. Barlow, M. Louie, R. Hao, P.A. Defnet, B. Zhang, Electrodeposited gold on carbon-fiber microelectrodes for enhancing amperometric detection of dopamine release from pheochromocytoma cells, Anal. Chem., 90 (2018) 10049-10055.
[69] H. Shinohara, Y. Sakai, T.A. Mir, Real-time monitoring of intracellular signal transduction in PC12 cells by two-dimensional surface plasmon resonance imager, Anal. Biochem., 441 (2013) 185-189.

Figure caption

Scheme 1. A) The schematic diagram of N-doped CMS and N-doped CHT. The hydrothermal treatment of glucose and thymine at 180 °C for 24h have been proceeded for forming the desired materials (a). The N-doped CMS was carbonized at 800 °C under N_2-flow (b). B) The control synthesis of N-doped CHT after mixing of glucose, thymine, and sodium dodecyl sulfate (SDS), then treated at high temperature (a), and carbonized at 800 °C under N_2-flow (b).

Figure 1. A) The FE-SEM images of N-doped MCS with low (a) and high magnification (b). B) The EDS-SEM of N-doped MCS for C (a), O (b), and N (c). C) The FE-SEM of N-doped OHCS with low magnification (a), high magnification (c), side view (c), and upper view (d). D) The EDS-SEM of N-doped OHCS for C (a), O (b), and N (c).

Figure 2. A) The Raman shift spectra of N-doped MCS (wine line) and N-doped OHCS (green line). B) The N_2-adsorption isotherm of N-doped MCS (wine line) and N-doped OHCS (green line). C) The NLDFT pore size distribution of N-doped MCS (wine line) and N-doped OHCS (green line). D) The WA-XRD of N-doped MCS (wine line) and N-doped OHCS (green line). The XPS survey of N 1S (E) and C 1S (F).

Figure 3. A) The CVs of IDA (a), N-doped MCS (b), and N-doped CHT (c) in the electrolyte solution of 0.1 M containing 1 mM KCl $[Fe(CN)_6]^{3-/4-}$ at scan rate of 100 mVs^{-1}. B) The EIS Nyquist plot of IDA (a), N-doped MCS/IDA (b), and N-doped CHT/IDA (c) in the electrolyte solution of 0.1 M containing 1 mM KCl $[Fe(CN)_6]^{3-/4-}$. C) The CVs of IDA (a), N-doped MCS (b), and N-doped CHT (c) in 100 µM NA (PB, pH = 7). D) The CVs of various NA-concentrations of 0, 100, and 200 µM (PB, pH = 7) on N-doped CHT/IDA.

Figure 4. A) The SWV measurements of various NA concentrations in the range of 0.01 – 0.3 µM on N-doped CHT/IDA (a). The calibration plot of [NA]/(µM) Vs the current (µA) at wide range of 0.01 – 0.3 µM (b). B) The chronoamperometry (CA) response of NA within dynamic injection of various concentrations from 0.01 to 2 µM at fixed applied potential of 0.27 V, under continuous stirring and N_2 flow (a). The calibration plot of

[DA]/(μM) Vs the current (μA) at wide range of 0.01 – 2 μM (b). The CA response of NA at low concentration range (c) and the calibration plot in the range of 0.01 – 0.1 μM (d).

Scheme 2. The schematic diagram of designing of the portable sensor based on N-doped CHT/IDA. A-C) The IDA design and fabrication for sensing of NA secreted from PC12 cells. D) The chipset connected to the potentiostate for recording the signal of NA.

Figure 5. The confocal microscopy image of PC12 cells incubated with the 100 μg/mL of N-doped CHT for bright field (A), phalloidin 488 for F-actine (B), DAPI for nucleus counter staining (C), and merged image (D). E) The column plot of N-doped CHT concentrations (μg/mL) versus the %cells viability using CCK-8 protocol and measured by microplate reader at 450 nm. E) The column plot of [K+]/mM versus the responded current (μA) of the released NA from PC12 cells

Scheme 1.

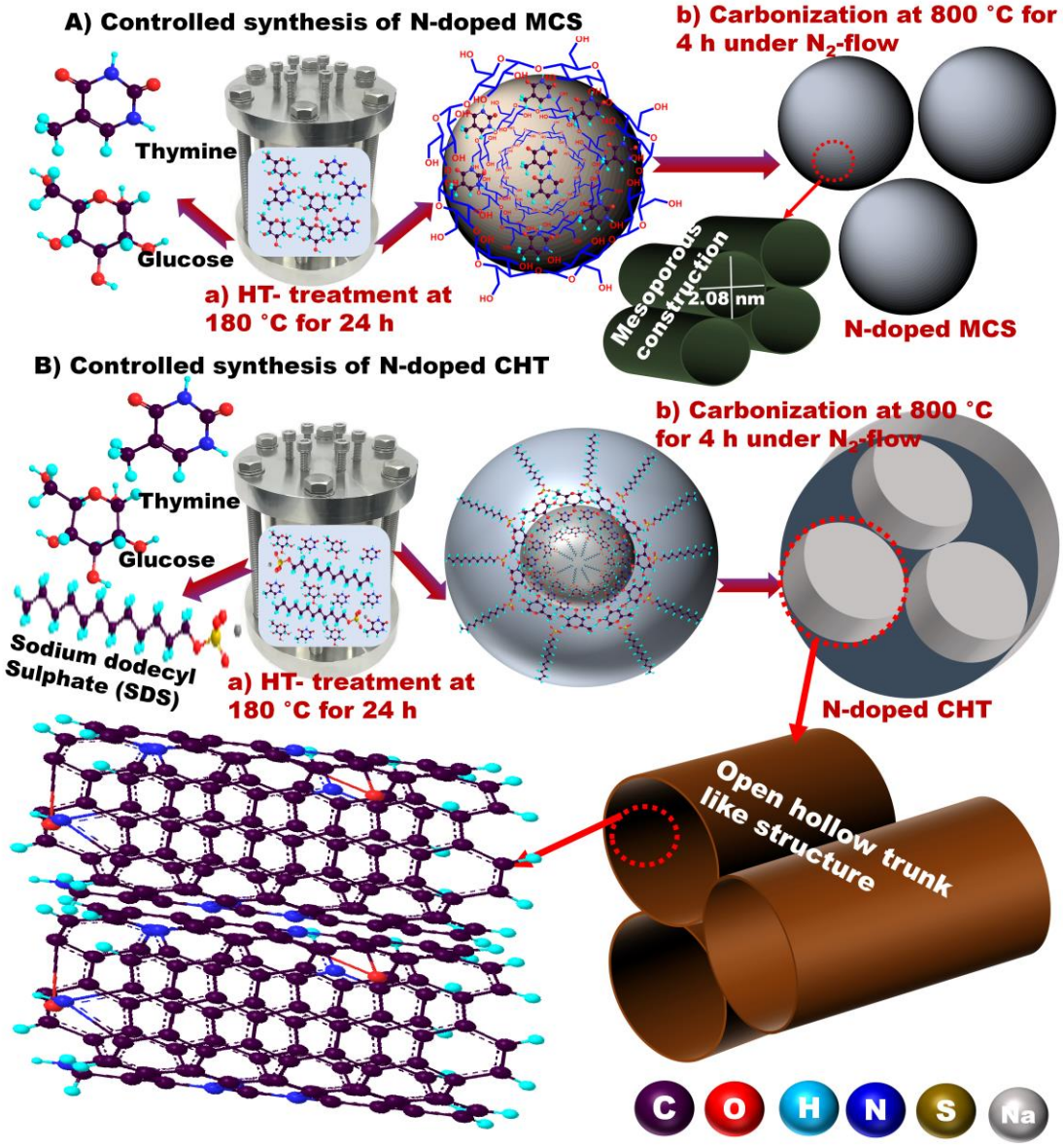
A) Controlled synthesis of N-doped MCS
b) Carbonization at 800 °C for 4 h under N_2-flow
Thymine
Glucose
a) HT- treatment at 180 °C for 24 h
Mesoporous construction
2.08 nm
N-doped MCS
B) Controlled synthesis of N-doped CHT
b) Carbonization at 800 °C for 4 h under N_2-flow
Thymine
Glucose
Sodium dodecyl Sulphate (SDS)
a) HT- treatment at 180 °C for 24 h
N-doped CHT
Open hollow trunk like structure
C
O
H
N
S
Na

Figure 1.

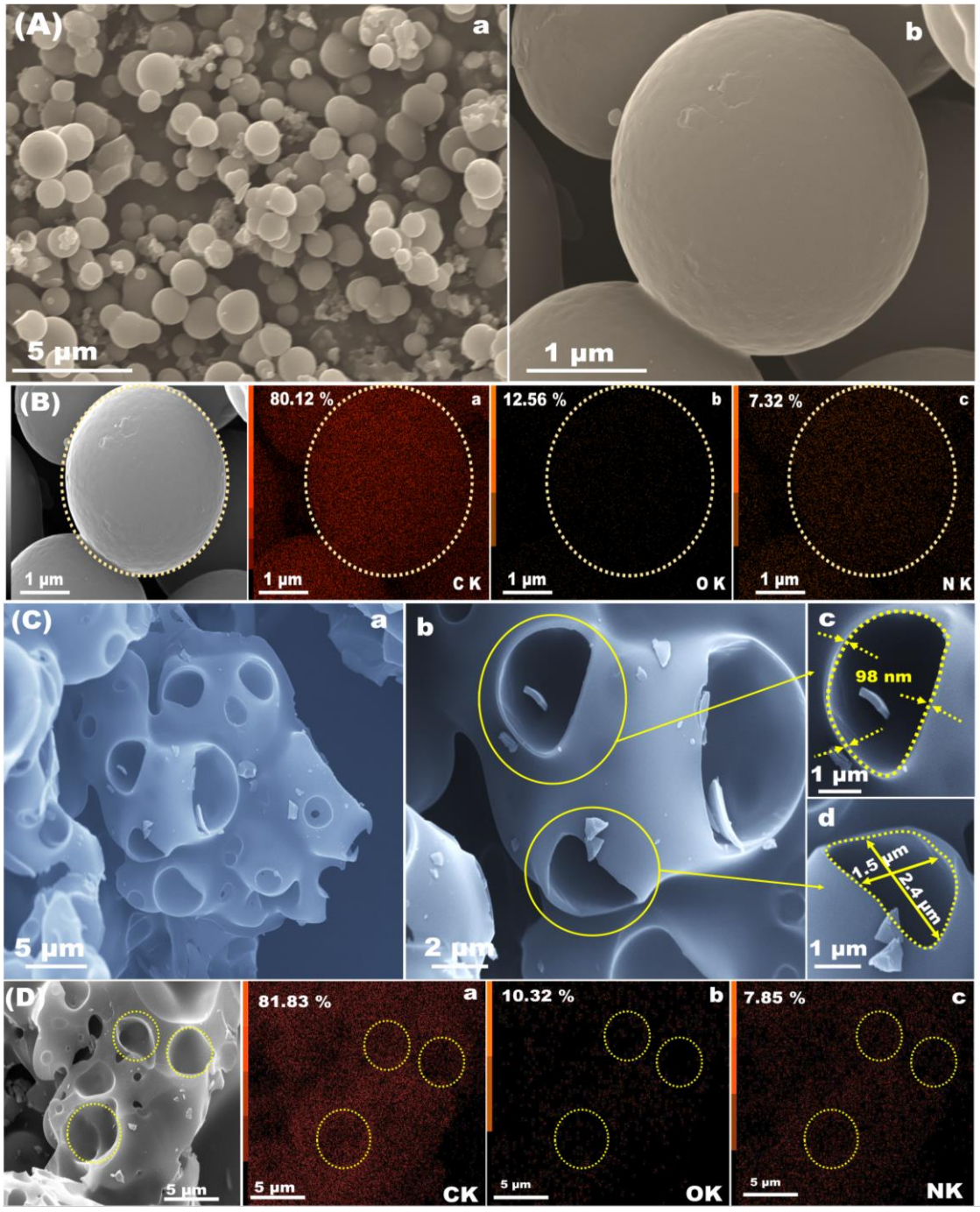
(A)
a
5 μm
b
1 μm
(B)
1 μm
80.12 %
a
1 μm
C K
12.56 %
b
1 μm
O K
7.32 %
c
1 μm
N K
(C)
a
5 μm
b
2 μm
c
98 nm
1 μm
d
1.5 μm
2.4 μm
1 μm
(D)
5 μm
81.83 %
a
5 μm
CK
10.32 %
b
5 μm
OK
7.85 %
c
5 μm
NK

Figure 2.

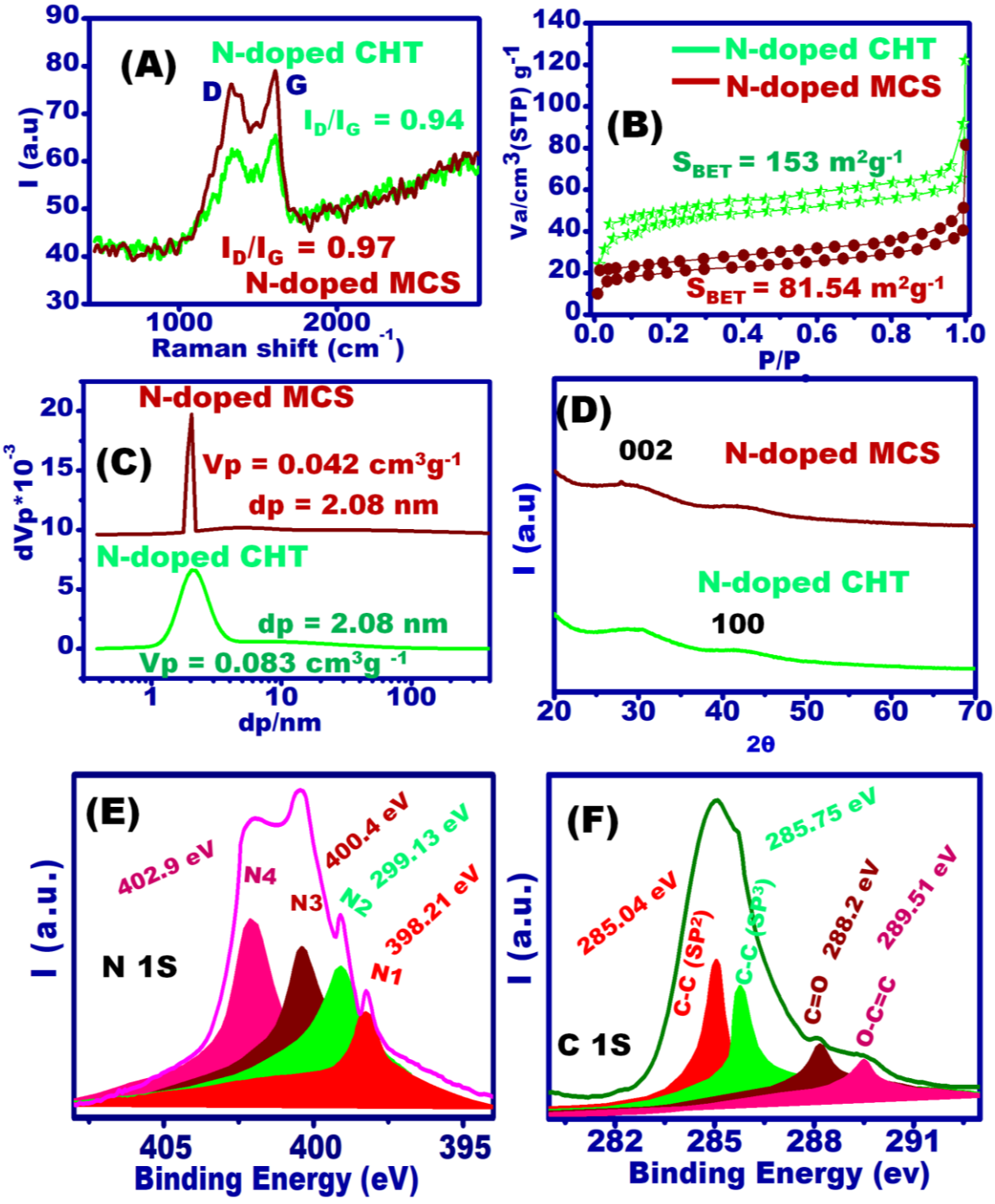
(A)
N-doped CHT
D
G
I_D/I_G = 0.94
I_D/I_G = 0.97
N-doped MCS
I (a.u)
Raman shift (cm^{-1})
(B)
N-doped CHT
N-doped MCS
S_{BET} = 153 m^2g^{-1}
S_{BET} = 81.54 m^2g^{-1}
Va/cm^3(STP) g^{-1}
P/P
(C)
N-doped MCS
Vp = 0.042 cm^3g^{-1}
dp = 2.08 nm
N-doped CHT
dp = 2.08 nm
Vp = 0.083 cm^3g^{-1}
dVp*10^{-3}
dp/nm
(D)
002
N-doped MCS
N-doped CHT
100
I (a.u)
2θ
(E)
402.9 eV
N4
N3
400.4 eV
N2
299.13 eV
398.21 eV
N1
N 1S
I (a.u.)
Binding Energy (eV)
(F)
285.75 eV
285.04 eV
C-C (SP^2)
C-C (SP^3)
288.2 eV
289.51 eV
C=O
O-C=C
C 1S
I (a.u.)
Binding Energy (ev)

Figure 3.

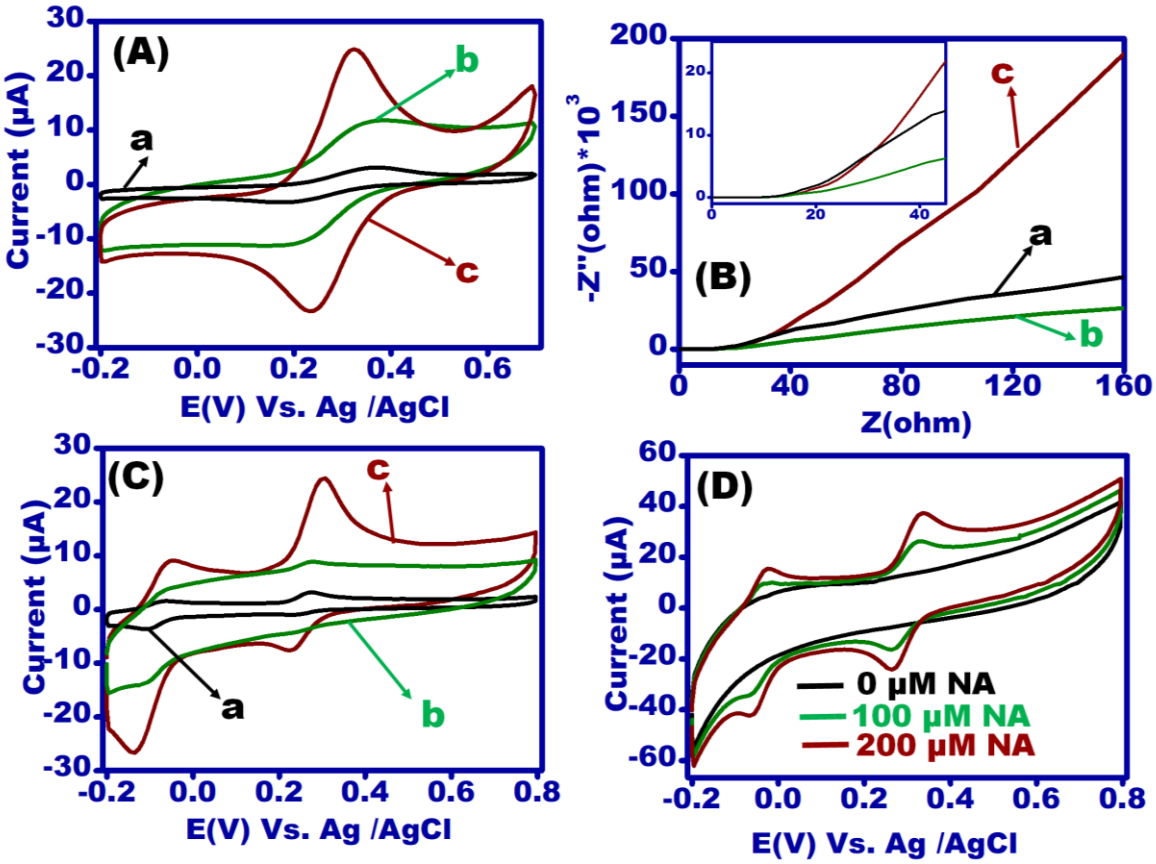
(A)
a
b
c
Current (μA)
E(V) Vs. Ag /AgCl
(B)
-Z''(ohm)*10^3
Z(ohm)
(C)
(D)
0 μM NA
100 μM NA
200 μM NA

Figure 4.

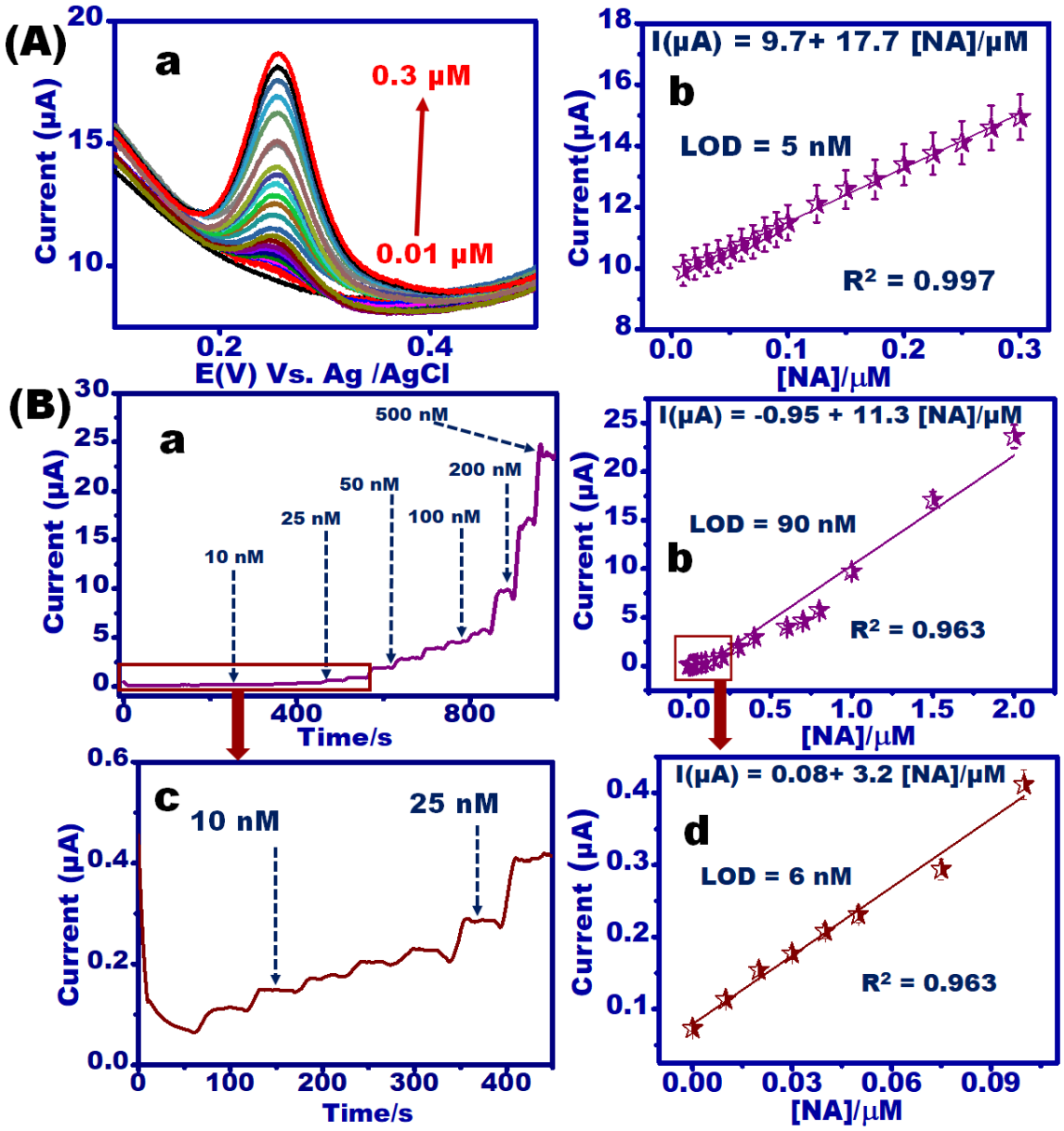
(A)
a
0.3 μM
0.01 μM
Current (μA)
E(V) Vs. Ag /AgCl
b
I(μA) = 9.7+ 17.7 [NA]/μM
LOD = 5 nM
R² = 0.997
Current(μA)
[NA]/μM
(B)
a
500 nM
200 nM
50 nM
25 nM
100 nM
10 nM
Current (μA)
Time/s
b
I(μA) = -0.95 + 11.3 [NA]/μM
LOD = 90 nM
R² = 0.963
[NA]/μM
c
10 nM
25 nM
Current (μA)
Time/s
d
I(μA) = 0.08+ 3.2 [NA]/μM
LOD = 6 nM
R² = 0.963
[NA]/μM

Scheme 2.

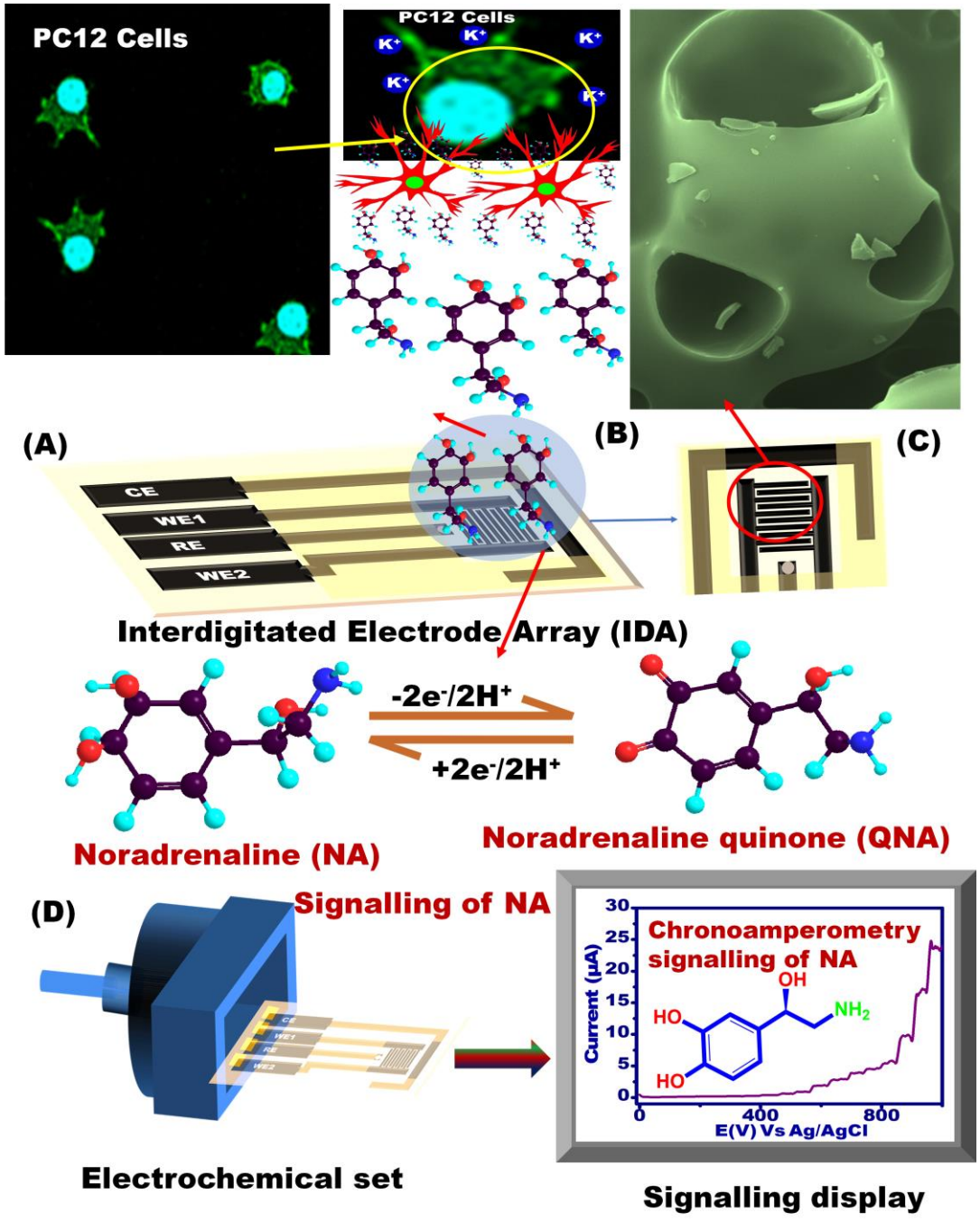
PC12 Cells
PC12 Cells
K+
(A)
(B)
(C)
CE
WE1
RE
WE2
Interdigitated Electrode Array (IDA)
-2e-/2H+
+2e-/2H+
Noradrenaline (NA)
Noradrenaline quinone (QNA)
(D)
Signalling of NA
Chronoamperometry signalling of NA
Current (µA)
E(V) Vs Ag/AgCl
OH
HO
NH2
Electrochemical set
Signalling display

Figure 5.

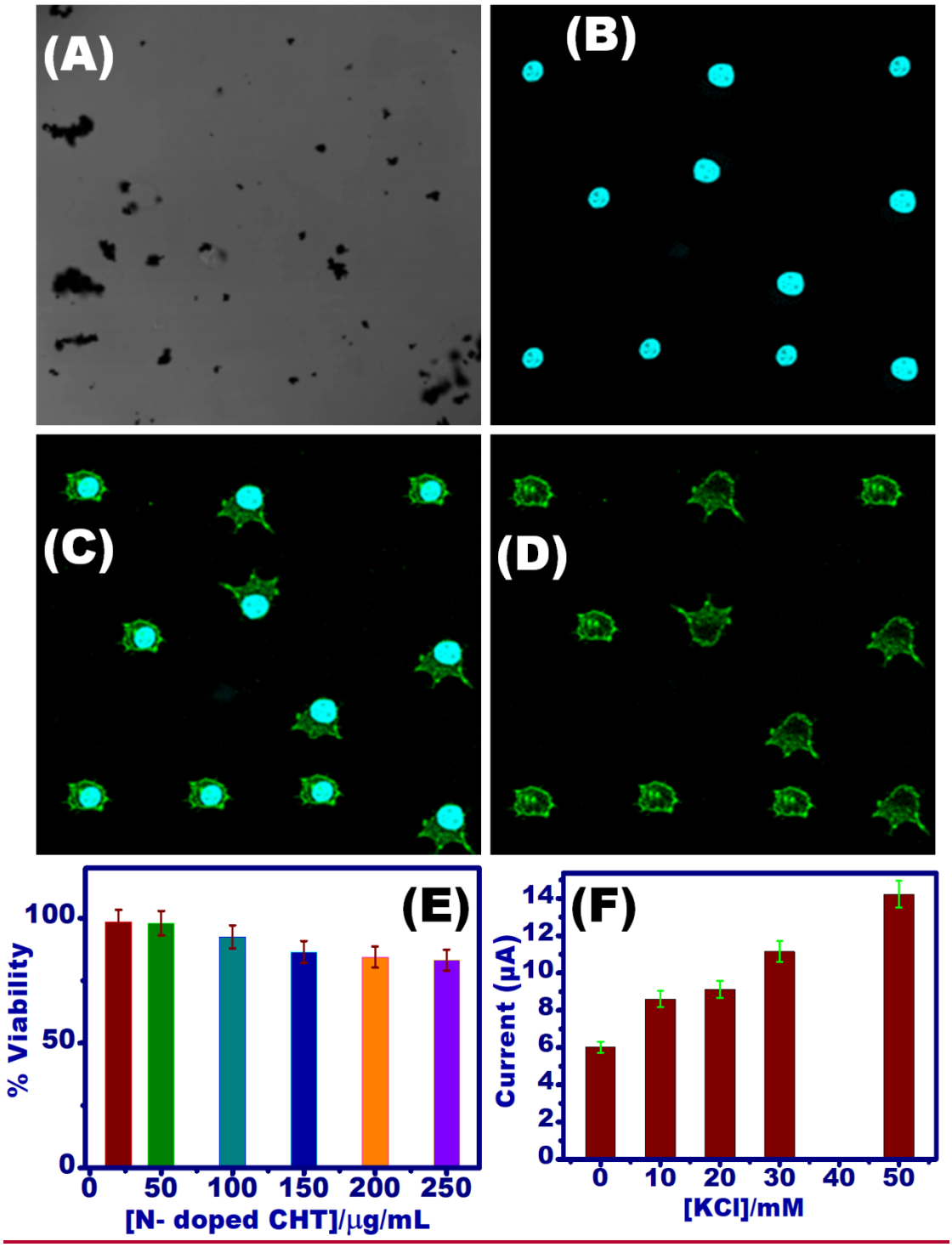
(A)
(B)
(C)
(D)
(E)
% Viability
100
50
0
0
50
100
150
200
250
[N- doped CHT]/μg/mL
(F)
Current (μA)
14
12
10
8
6
4
2
0
0
10
20
30
40
50
[KCl]/mM